Marine and Petroleum Geology 51 (2014) 230–238

Contents lists available at ScienceDirect

Marine and Petroleum Geology

journal homepage: www.elsevier.com/locate/marpetgeo

Modeling stress evolution around a rising salt diapir

Maria A. Nikolinakou [a,*], Peter B. Flemings [b], Michael R. Hudec [a]

[a] Bureau of Economic Geology, The University of Texas at Austin, 10100 Burnet Road, Building PRC-130, Austin, TX 78758, USA
[b] Jackson School of Geosciences, The University of Texas at Austin, 10100 Burnet Road, Building PRC-130, Austin, TX 78758, USA

ARTICLE INFO

Article history:
Received 2 July 2013
Received in revised form
15 November 2013
Accepted 29 November 2013
Available online 10 December 2013

Keywords:
Numerical modeling
Forward modeling
Salt diapir
Poro-elastoplasticity
Wellbore stability
Hoop stress

ABSTRACT

We model the evolution of a salt diapir during sedimentation and study how deposition and salt movement affect stresses close to the diapir. We model the salt as a solid visco-plastic material and the sediments as a poro-elastoplastic material, using a generalized Modified Cam Clay model. The salt flows because ongoing sedimentation increases the average density within the overburden sediments, pressurizing the salt. Stresses rotate near a salt diapir, such that the maximum principal stress is perpendicular to the contact with the salt. The minimum principal stress is in the circumferential direction, and drops near the salt. The mean stress increases near the upper parts of the diapir, leading to a porosity that is lower than predicted for uniaxial burial at the same depth. We built this axisymmetric model within the large-strain finite-element program Elfen. Our results highlight the fact that forward modeling can provide a detailed understanding of the stress history of mudrocks close to salt diapirs; such an understanding is critical for predicting stress, porosity, and pore pressure in salt systems.

1. Introduction

A significant number of hydrocarbon reservoirs around the world are found in layers dipping away from salt diapirs. As a result, the energy industry routinely drills near salt diapirs (Beltrão et al., 2009; Meyer et al., 2005; Seymour et al., 1993). This is an environment with significant stress perturbations, because the rising of the salt has imposed an additional load on adjacent sediments (Dusseault et al., 2004; Seymour et al., 1993). Indeed, many wells near salt diapirs have encountered drilling problems, leading to additional expense or even abandonment (Bradley, 1978; Dusseault et al., 2004; Willson et al., 2003).

The strength of sediments, as well as their response to external loading, is a function of their loading history since deposition (Terzaghi et al., 1996), and their diagenetic history (Laubach et al., 2010). Taking the stress history into account is especially critical in environments, such as those near salt diapirs that have undergone significant geologic loading. Hence, the current strength and stress state of the salt wall rocks will be more closely predicted when the development of the salt diapir is modeled concurrently with the basin sedimentation.

The evolution of salt diapirs has been studied extensively using kinematic restorations (Rowan and Ratliff, 2012). Such studies aim to explain the present-day geologic cross section through a sequence of plausible past sections without looking into stresses within the sediments. Similarly, large-strain numerical studies (Albertz and Beaumont, 2010; Albertz et al., 2010; Allen and Beaumont, 2012; Chemia et al., 2009; Goteti et al., 2012; Gradmann et al., 2009; Schultz-Ela, 2003) have focused on the geologic evolution of salt systems without modeling the geomechanical response of the wall rocks.

Over the last two decades, a number of studies employed a geomechanical approach to model salt-sediment interaction and improve understanding of stress changes around salt (Barnichon et al., 1999; Daudré and Cloetingh, 1994; Fredrich et al., 2003; Fullsack, 1995; Koupriantchik et al., 2005, 2004; Luo et al., 2012; Mackay et al., 2008; Nikolinakou et al., 2012; Orlic and Wassing, 2012; Poliakov et al., 1993a, 1993b, 1996; Sanz and Dasari, 2010; Schultz-Ela et al., 1993; van-der-Zee et al., 2011). Considerable progress has been recently achieved in this field (e.g., by the use of coupled poro-elastoplastic analyses to predict the transient pore pressure and stress changes around salt (Nikolinakou et al., 2012) or by three-dimensional simulations of actual salt structures, combined with poro-elastic formulations (van-der-Zee et al., 2011)). However, most published analyses have used simple or idealized salt geometries, and were not able to simulate the evolution of salt-diapir geometry.

* Corresponding author. Tel.: +1 512 471 0415.
E-mail addresses: mariakat@mail.utexas.edu, mariakat@alum.mit.edu (M.A. Nikolinakou), pflemings@jsg.utexas.edu (P.B. Flemings), michael.hudec@beg.utexas.edu (M.R. Hudec).

0264-8172/$ – see front matter © 2013 Elsevier Ltd. All rights reserved.
http://dx.doi.org/10.1016/j.marpetgeo.2013.11.021

Here, we simulate the rising of a salt diapir within a sedimentary basin and we model the wall rocks as porous elastoplastic materials. Our study offers two major achievements distinct from previous work on salt-diapir and sediment interaction:

a) We simulate sedimentation simultaneously with the movement of the salt. This means that the stresses within the basin develop as a function of both the depositional process and the loading from the salt. Such a simulation is a significant advance compared to traditional basin models (Althaus, 1977; Jaeger et al., 2007; Pilkington, 1978; Turcotte and Schubert, 2002), which assume that the vertical stress is the maximum principal stress and equal to the overburden, and that the horizontal stresses are a ratio of the vertical (estimated, for example, by empirical correlations (Matthews and Kelly, 1967) or the frictional resistance of normal faulting (Zoback and Healy, 1984)). Consequently, the porosity–depth profile in our model differs from that of a basin that has been uniaxially deposited; here, the porosity–depth profile has been modified by the action of the salt.
b) The movement of the salt itself is not prescribed. The salt diapir is rising and expanding because of increasing basin weight (due to sedimentation). Hence, the salt diapir rise is coupled with the sedimentation process, in the sense that sedimentation is causing the salt to deform, which, in turn, changes the stresses within the depositing wall rocks.

Our analysis shows that stresses rotate near a salt diapir, such that the maximum principal stress is perpendicular to the contact with the salt. The minimum principal stress is in the hoop direction, and drops near the salt, resulting in a reduced range of acceptable drilling mud weights. The mean stress increases near the upper parts of the diapir, leading to a porosity that is lower than predicted for uniaxial burial at the same depth.

2. Finite-element model

We built our numerical model within the finite-element program Elfen® (Rockfield, 2010). This forward-modeling technology uses a finite strain quasi-static, explicit, Lagrangian finite-element formulation, complemented by automated adaptive remeshing techniques. It can simulate sedimentation and includes computational features developed for the modeling of salt diapirs (Peric and Crook, 2004; Thornton et al., 2011).

We study the evolution of a three-dimensional salt diapir using an axisymmetric model (360^0 rotation of the vertical section shown in Fig. 1). Because the structure is axisymmetric, all horizontal sections are circular. Initially, the salt is 12 km thick at the center of the diapir ($r = 0$, Fig. 1) and 6 km at the outer edge ($r = 20$ km). The initial sediment basin is 6.25 km thick at the far-field boundary ($r = 20$ km). 250 m of sediment buries the top of the salt diapir. There is no slip between the diapir and the basin. The base and side boundaries are rollers (zero-normal-displacement, free-slip boundaries), and the model is wide enough that the side boundary is unaffected by any stress perturbations. The initial stresses in the model are geostatic, with a horizontal-to-vertical effective stress ratio of $K_0 = 0.8$. Pore pressures are assumed hydrostatic and do not change during the analysis (drained simulation). We simulate sedimentation by aggrading the top of the model 400 m every half million years. The local thickness of the aggraded layer depends on the surface topography prior to sedimentation.

We model the salt as a solid viscoplastic material using a reduced form of the Munson and Dawson formulation (the transient term is omitted as negligible over geological time scales and only the two steady-state terms are included) (Munson and Dawson, 1979). This is a constitutive model that provides a unified approach to both creep and plasticity and is formulated such that the salt viscosity is a function of both effective stress and temperature. The formulation has a series of input parameters (Appendix A, Table A.1), that are calibrated according to (Fredrich et al., 2007; Munson, 1997); the density is constant and equal to 2200 kg/m^3, and the equivalent salt viscosity varies between 10^{18}–10^{20} Pa s. Basin sediments are modeled as porous elastoplastic, using the SR3 constitutive model from the Elfen® material library (Rockfield, 2010). SR3 is a critical state formulation that is based on the principles of Modified Cam Clay (Muir Wood, 1990). The model is a single-surface, rate-independent, non-associative, elastoplastic model (Crook et al., 2006; Rockfield, 2010). The input for the model parameters has been calibrated using experimental data by Nygard et al. (2006, 2004) (Appendix A, Table A.2). The density varies with depth as a function of porosity; Figure 1 shows the density variation within the basin at the initial stage. During the simulation, porosity changes because of the sedimentation and of the salt-diapir rise; as a result, the density of the sediments is also updated.

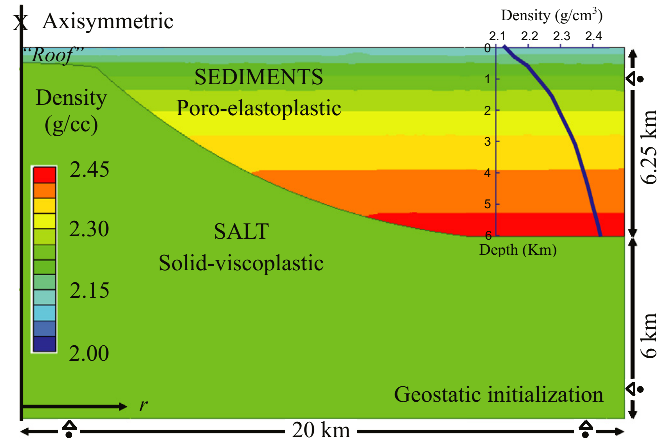

Figure 1. Plane of revolution for axisymmetric numerical model (vertical section). Initial dome has height of 12 km at center, whereas basin reaches 6.25 km depth at far end of model ($r = 20$ km). Contours and inset plot show density–depth profile of initial section.

The finite-element mesh is composed of unstructured quadrilaterals with an initial element size of that varies from 300 m in the far field, to 100 m at the top of the diapir. Adaptive remeshing is allowed in the top-central part of the salt diapir, and it is activated after a threshold plastic strain has been reached.

3. Mechanism of salt flow

The diapir-basin system is in static equilibrium when the weight of the overburden is the same across any given horizontal section. In order to achieve this equilibrium, the weight of the salt diapir needs to be equal to the weight of the basin, or:

$$\rho_{\text{salt}} gz + \sigma_{v,roof} = \int \rho_{sed} gz \mathrm{d}z \tag{1}$$

where z is the depth, ρ_{salt} is the density of the salt (2200 kg/m^3), ρ_{sed} is the density of the sediments at depth z, $\sigma_{v,roof}$ is the weight of the salt roof, and g the acceleration of gravity (see Appendix B for definition of all variables). As new sediments are deposited on top of the model, the mass-column-balance is temporarily disrupted.

We consider, for example, the model after 2 m.y. of sedimentation (Fig. 2a). At this time, the upper parts of the diapir have

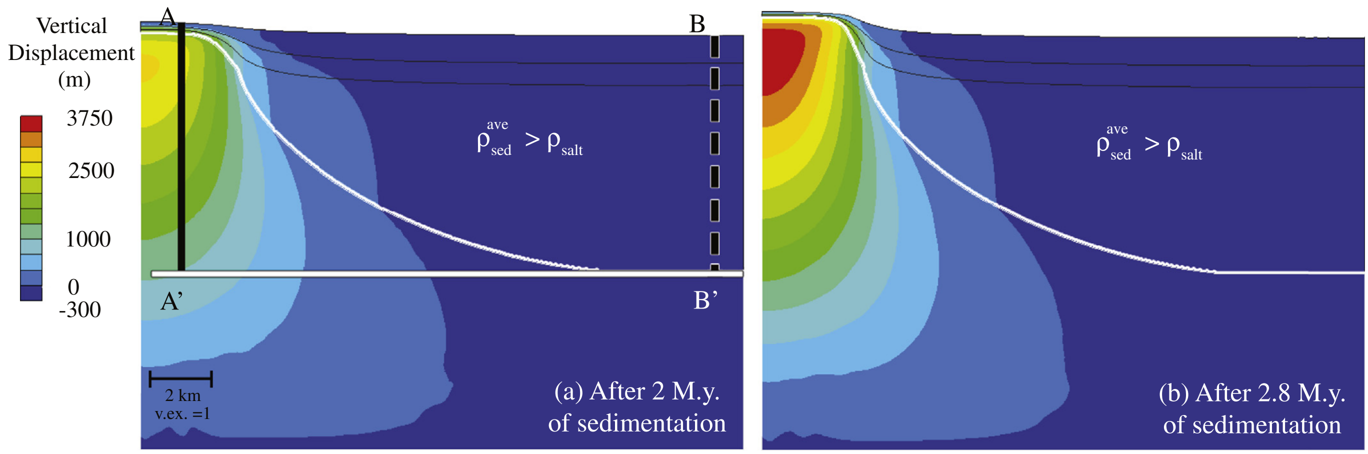

Figure 2. Vertical sections showing salt geometry after a) 2 m.y. of sedimentation (left); and b) additional 0.8 m.y. with no sedimentation (right). Contours show accumulated vertical displacement since beginning of simulation. In order for horizontal white section to be in equilibrium, weight of salt needs to be equal to weight of basin; achieved with increased salt height (right).

already moved upwards more than 2500 m (Fig. 2a). Because the density of the salt is less than the average density of the sediments, the horizontal section highlighted in Figure 2a is not in equilibrium. Salt will only balance the weight of the basin if the salt becomes heavier by increasing its height. Indeed, if we stop the sedimentation process, the simulation evolves without any external loading force, and asymptotically reaches a static equilibrium after about 1 m.y. (Fig. 2b). During this time, the center of the salt diapir rises by an additional 1000 m, and the weight contributed by this upwards-vertical movement succeeds in balancing the integrated weight of the sediment basin (Fig. 2b). In other words, the salt flows until the height of the diapir is sufficient to balance the weight of the sedimentary basin. Because, in this case, the average sediment density is greater than that of the salt, the basin sinks and the salt diapir rises.

Another way to represent the driving force for salt flow is to examine the integrated far-field basin overburden at a given elevation. Figure 3 plots vertical stress profiles through the diapir

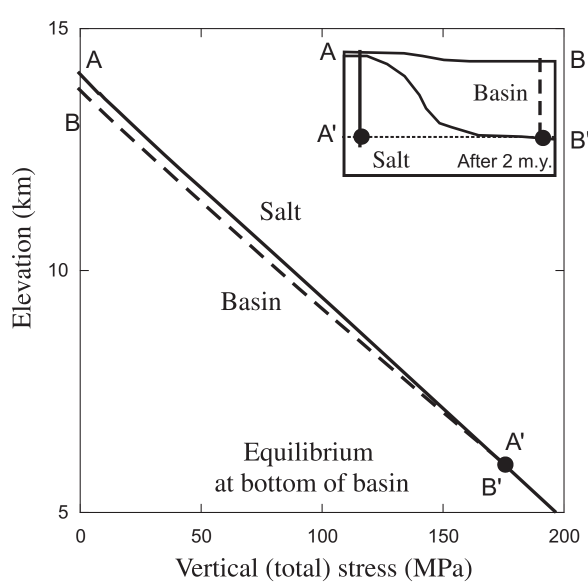

Figure 3. Vertical stress profiles through dome and far-field basin, after 2 m.y of sedimentation (profile locations shown Fig. 2). Stresses become equal at bottom of basin.

and the basin (away from the salt diapir). The salt pressure is higher, because the topographic surface has a higher elevation above the salt diapir. However, the salt stress has a lesser gradient, and becomes equal to the far-field basin overburden at the elevation of the sediment base. The higher stress within the salt, despite the fact that the salt density is lower than the average density of the sediments, indicates that the salt is loaded beyond its overburden value. We define as salt *overpressure* the difference between the measured salt stress and the integrated overburden at any given depth:

$$\sigma_{op,salt} = \sigma_{v,salt} - \left(\rho_{\text{salt}} g z + \sigma_{v,roof}\right) \tag{2}$$

where $\sigma_{v,salt}$ is the measured stress within the salt, and $\sigma_{op,salt}$ is the salt overpressure. Even though salt is modeled as a solid material, the term *overpressure* is used here to indicate stresses in excess of the halostatic, similar to fluid pressures in excess of the hydrostatic. The salt overpressure increases with depth (Fig. 4) and provides the potential for salt flow. Indeed, the vectors of the salt flow are perpendicular to the contours of the salt overpressure (Fig. 4).

4. Stresses within the wall rocks with combined sedimentation

When modeling sedimentation for a total duration of 5 m.y., the salt diapir rises by a total of 4.7 km (Fig. 5). The sedimentation process is coupled to the movement of the salt body, and, at the same time, the salt flow changes the stresses within the basin sediments (contours of vertical stress on Fig. 5).

4.1. Deformation pattern and stress changes

Rise of a salt diapir loads its wall rocks, because the salt expands out as it moves up (Fig. 6). In the circumferential (hoop) direction, the diapir expands outwards, leading to an increase in the radius of any horizontal diapir section (Fig. 6). This can be quantified by the hoop strain, which reaches values up to 80% at the upper parts of the diapir. Owning to the significant stretching in the horizontal plane, the hoop (or circumferential) stress within the adjacent sediments decreases in comparison to the far-field horizontal/hoop stress (Fig. 7b).

The salt diapir is pushing outwards, subjecting the wall rocks to a horizontal compression (Fig. 7a). This increases the

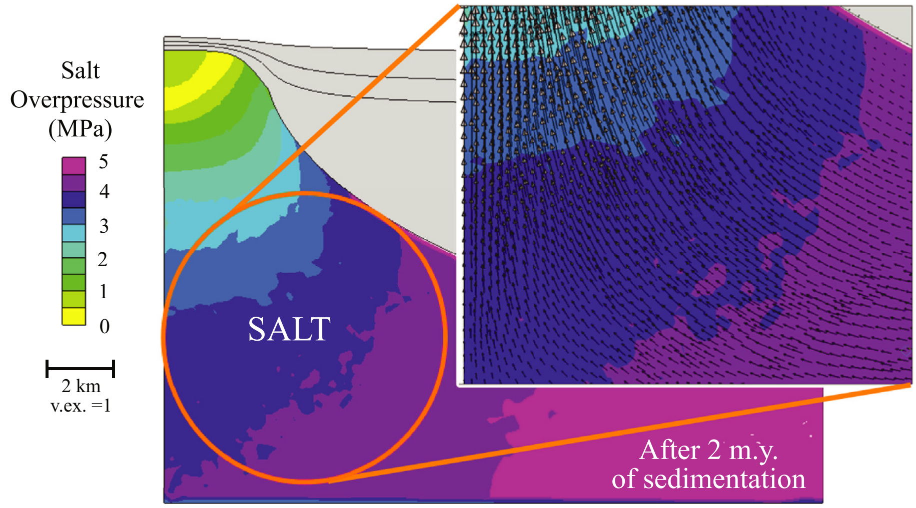

Figure 4. Vertical section showing contours of salt overpressure. Salt overpressure is defined as difference between measured salt stress and integrated salt overburden at any given depth. Arrows show direction of salt flow, and they are normal to overpressure contours, indicating that excess pressure within salt provides potential for salt flow.

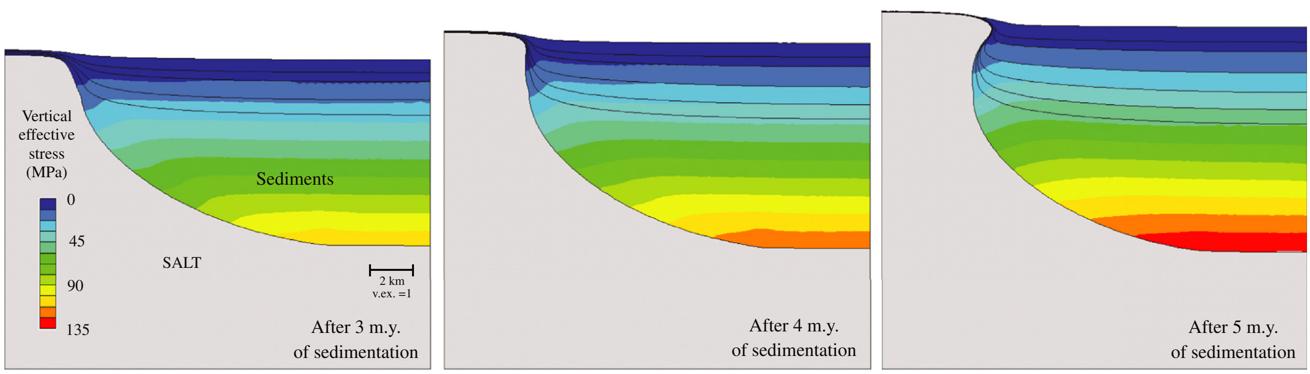

Figure 5. Vertical sections predicted by the numerical model after 3, 4, and 5 m.y. of sedimentation. Contours illustrate changes in vertical stress due to sedimentation and simultaneous salt movement.

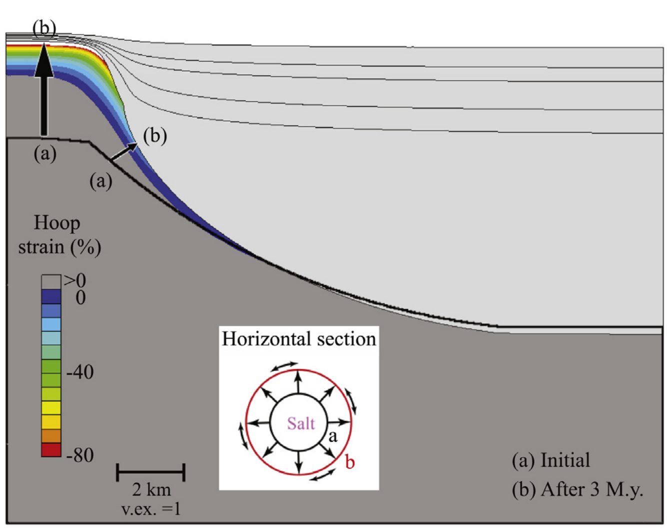

Figure 6. Vertical section showing salt geometry at beginning of simulation, and after 3 m.y. of sedimentation. Contours show extensional hoop strain accumulated during simulation. Inset map-view sketch illustrates that in circumferential direction the dome expands outwards, leading to increase in radius of any horizontal dome section.

horizontal stress (green solid line in Fig. 7b) above its far-field value (dotted gray line) and to values even higher than the integration of the overburden (dashed gray line) close to the upper parts of the diapir. On the other hand, the vertical stress (dotted solid purple line in Fig. 7b) decreases in the sediments next to the salt diapir.

4.2. Principal stresses next to a rising salt diapir

The decrease of the vertical stress near the salt diapir to less than the overburden stress is associated with the rotation of the principal stresses within the wall rocks, which reflects the requirement for strain compatibility along the salt-sediment interface: The salt, being a viscoplastic material, is characterized by a very low shear stress, so that all stresses within the salt are nearly equal. Since no slip is possible between the salt and the basin sediments in the model, the near-isostatic state of the salt mandates the rotation of the principal stresses in the wall rocks such that they become perpendicular and tangential to the contact with the salt diapir. As the salt is approached, the maximum principal stress (σ_1) becomes perpendicular to the salt face and increases to a value equal to the stress inside the salt (Fig. 8). At the far field, where the contact with the salt is horizontal, the vertical stress is the major principal stress, and it is equal to the overburden value. Close to the upper, vertical faces of the diapir, the maximum principal stress is horizontal (and higher than the overburden

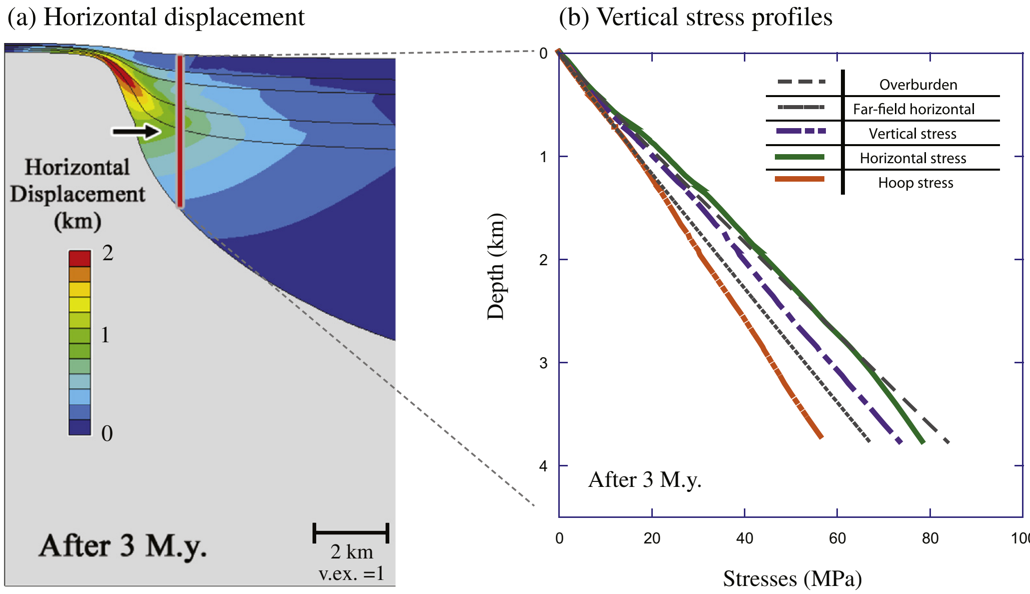

Figure 7. (a) Vertical section with contours of horizontal displacement next to rising salt dome, after 3 m.y. of deposition; (b) Stress profiles of horizontal, vertical, and hoop stresses along well next to salt. Hoop horizontal stress notably lower than far-field horizontal stress value; radial horizontal stress significantly increased compared to far-field value, and higher than overburden value near top parts of salt dome. Vertical stress less than overburden value.

value, Fig. 7b). Along the curved part of the contact, the principal stresses have rotated so that neither vertical nor horizontal are principal directions. In this case, the weight of overburden is supported by the salt via the maximum principal stress, through arching.

The direction of the maximum principal stress is always perpendicular to the salt, but the minimum principal direction switches between the two tangential stresses (the hoop stress in the horizontal plane and the tangential stress in the vertical plane, Fig. 8). In the basin sediments close to the contact with the salt, the minimum principal stress is in the circumferential (hoop) direction from the diapir center out to a distance of $r = 9$ km (thick dotted line superimposed along the salt contact in Fig. 8). This configuration results from the circumferential expansion of the diapir during its rise, which decreases the hoop stress close to the diapir (Fig. 7b, double-dotted solid orange line).

4.3. Changes in the mean stress and porosity

The mean stress (average of the three principal stresses) near a salt diapir is affected by two opposing stress changes: a) significant increase in the horizontal stress, especially at the upper parts of a salt diapir, where the wall is vertical and the salt is pushing out; and b) decrease in both the vertical and the hoop stresses, because of the stress rotation near the diapir and the expansion of the salt (plan view, Fig. 6). The combination of these stress changes leads to a net increase of the mean stress close to the upper parts of the diapir, and a decrease near the base of the diapir, compared to the far-field values at the same depth (Fig. 9).

Consequently, the porosity near the vertical parts of the salt diapir is lower than the porosity predicted by a uniaxial consolidation model for the same depth (Fig. 10); the sediments around the top of the diapir have been consolidated locally to a higher stress level. Near the base of the diapir, the decrease in the mean stress is associated with a porosity that is higher than the far-field value at the same depth, and the wall rocks have been locally unloaded.

5. Discussion

We have simulated the formation of a salt diapir without kinematically prescribing the salt and while representing the sediments using a poro-elastoplastic formulation.

In contrary to traditional basin models, which assume that the vertical stress is equal to the weight of the overburden and that the horizontal stress can be obtained as a ratio of the vertical, the stresses in our model develop as a function of the deposition process, as well as the salt loading. As a result, we obtain vertical stresses that are less than the overburden value, and radial horizontal stresses that are higher than the overburden around the upper parts of the diapir (Fig. 7). Furthermore, we predict the existence of areas in the wall rocks next to the diapir that have porosities lower than what a basin model would calculate (Fig. 10).

Our results also show that the minimum principal stress next to the rising salt diapir is in the circumferential (hoop) direction. This orientation of the minimum principal stress suggests that radial normal faults should be favored near the diapir, as is commonly observed (Davison et al., 2000; O'Brien and Lerch, 1987; Stewart, 2006). The predicted decrease in the hoop stress also means that the fracture gradient is reduced near the diapir; in practice, this suggests a narrower range of admissible mud weights for drilling near a salt diapir (Fig. 11).

Numerous systems need to be studied to completely understand the stress changes caused by a rising salt diapir. One should model the coupled development of pore pressures, as well as the presence of an initial thrust environment ($K_0 > 1$). Sensitivity analyses are needed to understand the effect of initial salt geometries and the relationship between sedimentation rates and rheological properties of salt. Furthermore, there is little understanding on how stresses change when the root salt thins out and/or welds and when the salt diapir evolves into an advancing salt sheet.

The current study represents the first example that couples sedimentation with salt rise and captures the porous elastoplastic response of basin mudrocks. Nonetheless, our results provide a mechanical explanation for some of the observed stress perturbations around salt diapirs.

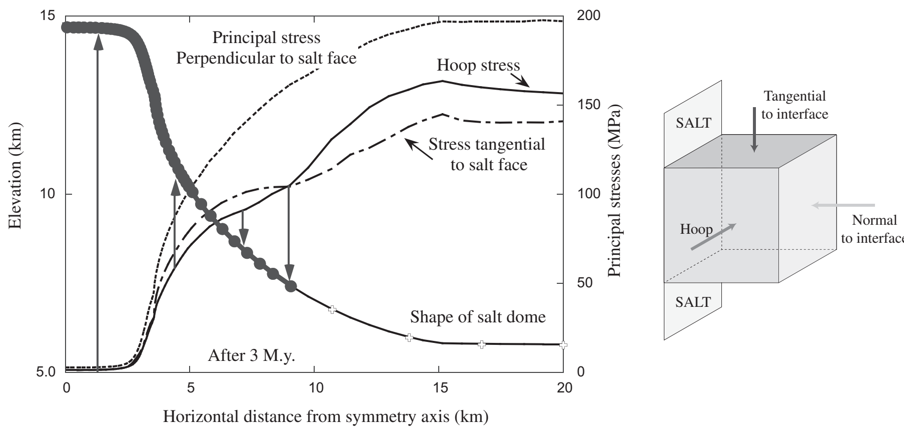

Figure 8. Location of salt-sediment interface after 3 m.y. of sedimentation (elevation given by left vertical axis), and principal stresses at all points along salt interface (stress values given by right vertical axis). Although maximum principal stress is always perpendicular to salt face, minimum and intermediate principal stresses change direction at distance $r = 9$ km from center of dome. Minimum principal stress in circumferential (hoop) direction everywhere along salt-sediment contact up to radial distance of $r = 9$ km from center of dome (thick dotted line).

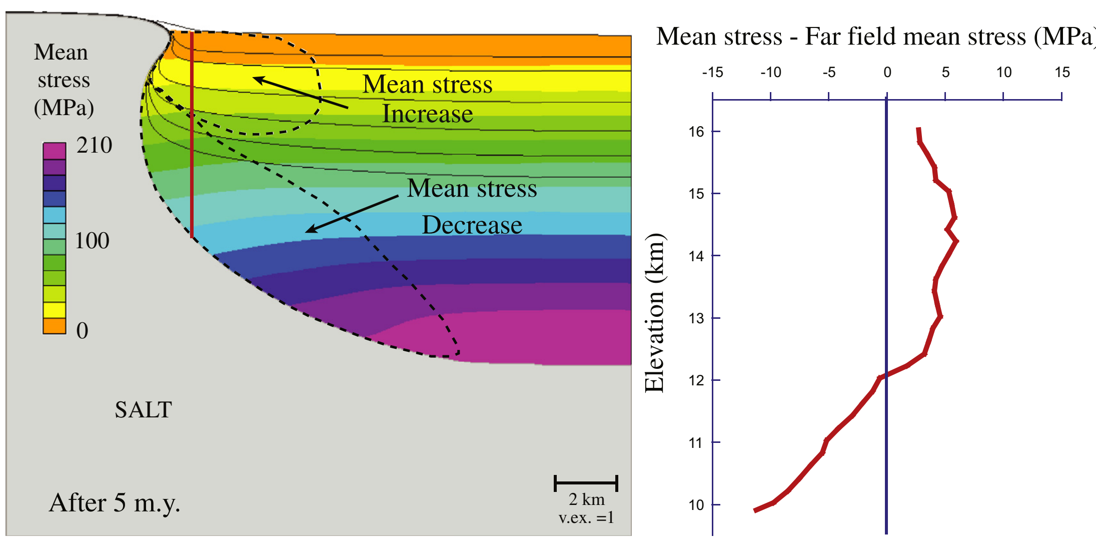

Figure 9. Vertical section showing mean stress contours near rising salt dome after 5 m.y. of deposition (left), and stress profile along vertical well plotting difference between the mean stress minus far-field mean stress.

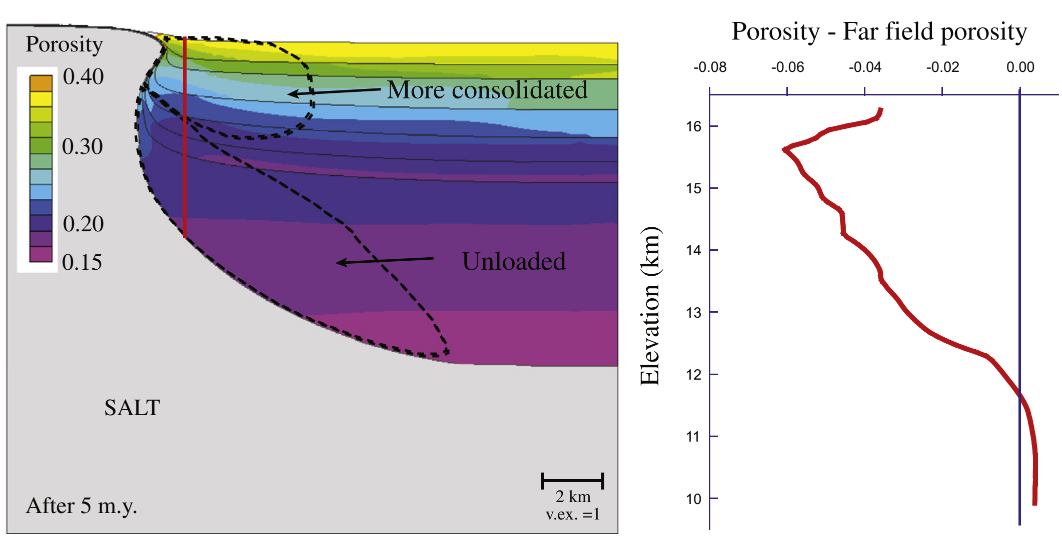

Figure 10. Vertical section showing porosity contours in wall rocks next to rising salt dome. Close to upper parts of the dome, where salt is pushing outwards, sediments have lower porosity than value predicted by uniaxial consolidation assumptions.

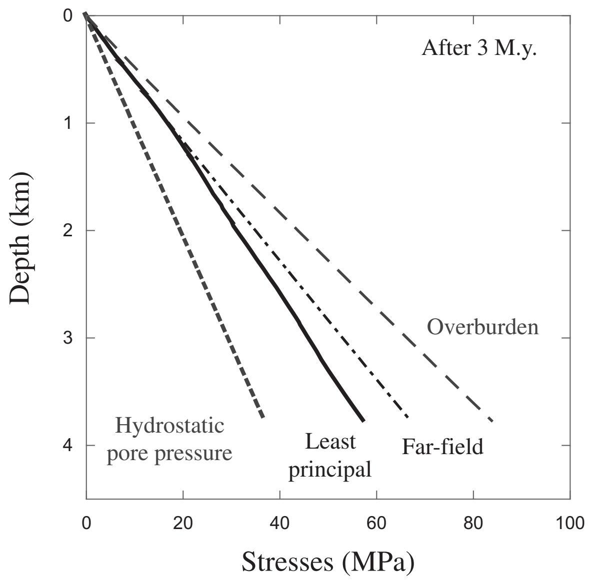

Figure 11. Stress profiles of least principal stress along vertical well after 3 m.y. of deposition, illustrating reduced admissible range of drilling mud weights next to dome (well location same as in Fig. 7a).

Reduced stress values at the circumferential (hoop) direction are often reported near salt diapirs and such stresses are associated with borehole instabilities and loss of circulation. Bradley (Bradley, 1978) discusses borehole instabilities near a salt diapir at Eugene Island, attributing them to a significantly lowered hoop stress near the flank of the diapir. Dusseault et al. (2004) report that initial drilling of an anticlinal structure above a Gulf of Guinea salt diapir in the 1990's resulted in 92 lost drilling days because of an exceptionally low minimum principal stress value, a mud window less than 0.05 density units, and massive lost circulation. The authors argue that this reduced minimum principal stress is in the circumferential direction, and discuss the analogy between salt diapirs and rising igneous intrusions, which also impose strains that lower the hoop stress (e.g., the Spanish Peaks in the Raton Basin, South Colorado, or the Sweetgrass Hills near the Alberta border in Montana (Dusseault et al., 2004)). Seymour et al., (Seymour et al., 1993) also attribute borehole instabilities near a salt diapir to a significantly lowered hoop stress near the flanks, and note that these problems led to a nonproductive drilling time of 26.3%. Our model shows that during the rising process, the salt diapir is expanding in the circumferential direction and, as a result, imposing high extensional strains on the wall rocks; therefore, the hoop stress should be expected to drop near salt diapirs, leading to a smaller range of admissible mud weights.

Several authors note that the principal stresses rotate near a salt diapir (Bachrach et al., 2007; Dusseault et al., 2004; Zerwer, 1994). According to standard practice (Bradley, 1978; Perez et al., 2008), wells drilled through salt should exit the salt perpendicular to the salt/sediment interface, which echoes the fact that the maximum principal stress rotates to be perpendicular to this interface. Dusseault et al. (2004) discuss the fact that, near the top flanks of a salt diapir, the maximum principal stress is horizontal and oriented radially, while the intermediate stress is vertical. The authors further note that the value of the maximum principal stress is equal to that of the overburden. Bradley (1978) also relates borehole collapse incidents at the side of a diapir to in-situ stresses that were higher than predicted. Our model predicts that the maximum principal stress is radial around the upper parts of the diapir, and furthermore, that it reaches values even higher than the weight of the overburden. Furthermore, the significant increase in the radial horizontal stress leads to an elevated mean stress near the upper parts of the diapir. As a result, our model predicts porosities that are lower than predicted for uniaxial burial at the same depth. Indeed, denser sediments have been observed near the "shoulders" of salt diapirs in the North Sea (Dusseault et al., 2004). Finally, observed radial and polygonal fault patterns suggest that the minimum principal stress lies in the circumferential direction (Davis et al., 2000; Dusseault et al., 2004). Indeed, our model shows that for a distance larger than the radius of the diapir, the hoop stress is the minimum principal.

6. Summary

We present an evolutionary numerical model of basin sedimentation and simultaneous salt diapir rising. We study the wall rocks as poro-elastoplastic materials and show that the minimum principal stress is in the circumferential direction and drops near the salt, resulting in a reduced range of admissible mud weights. We also show that the mean stress increases near the upper parts of the diapir, leading to a porosity lower than the one predicted by uniaxial basin modeling.

Comparison with published observations of stresses around salt diapirs shows that our evolutionary approach can improve predictions of stresses, possible fault directions, shear/tensile strength, and material properties (porosity, anisotropy in velocities measurements) in the wall rocks near a salt diapir.

Acknowledgments

The project was funded by the Applied Geodynamics Laboratory consortium and The University of Texas at Austin (U.T.) GeoFluids consortium. AGL is supported by the following companies: Anadarko, Apache, BHP Billiton, BP, CGG, Chevron, Cobalt, ConocoPhillips, Ecopetrol, ENI, ExxonMobil, Fugro, Global Geophysical, Hess, Ion, KNOC, McMoRan, Maersk, Marathon, Murphy, Nexen, Noble, Pemex, Petrobras, PGS, Repsol, Samson, Saudi Aramco, Shell, Statoil, Talisman, TGS, Total, Western Geco, and Woodside. U.T. GeoFluids is supported by the following companies: Anadarko, BHP Billiton, BP, Chevron, Conoco-Phillips, ExxonMobil, Hess, Schlumberger, Shell, Statoil and Total. The authors received additional support from the U.T. Jackson School of Geosciences. The text was edited by Chris Parker. Publication authorized by the Director, Bureau of Economic Geology.

Appendix A. Material input

Table A.1
Input material parameter values for the Munson–Dawson model (Fredrich et al., 2007; Munson, 1997; Munson and Dawson, 1979).

Parameter	Units	Value
E	MPa	10,000
ν	–	0.35
ρ	kg/m^3	2200
A_1	1/sec	1.885E+36
n_1	–	5.5
Q_1	cal/mol	25,000
A_2	1/sec	2.17E+26
n_2	cal/mol	5.0
Q_2	–	10,000
R	cal/°C/mol	1.987
T_0	°C	10
T_{CONST}	°C	273
G_0	MPa	12,400
dG/dT	GPa/°K	10.0

Table A.2
Input material parameter values for the SR3 model (Nygard et al., 2006, 2004; Rockfield, 2010).

Parameter	Units	Value
E	MPa	40
ν	–	0.25
ρ	kg/m^3	Figure 1
K_0	MPa	10
κ	–	0.01
$p_{t,0}$	MPa	0.085
$p_{c,0}$	MPa	−1.00
β	Degrees	60.00
ψ	Degrees	51.00
β_0	–	0.60
β_1	1/MPa	0.725
α	–	0.25
N	–	1.3
n_0	–	0.38
Hardening properties		Figure A.1

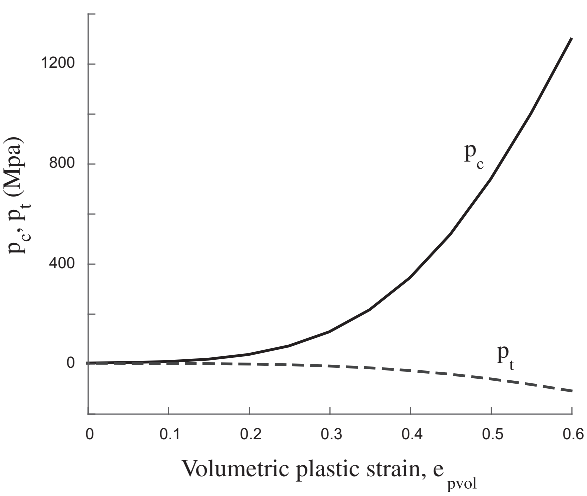

Figure A.1: Input Hardening properties for SR3 (Rockfield, 2010).

Appendix B

Table B.1
Nomenclature.

Symbol	Name	Dimensions
E	Elastic (Young's) Modulus	$L^{-1}M^1T^{-2}$
g	Acceleration of gravity	$L^1M^0T^{-2}$
r	Radial distance from the center of the model	$L^1M^0T^0$
z	Depth	$L^1M^0T^0$
η	Viscosity	$L^{-1}M^1T^{-1}$
ν'	Poisson's ratio	$L^0M^0T^0$
ρ_{salt}	Density of salt	$L^{-3}M^1T^0$
ρ_{sed}	Density of sediments	$L^{-3}M^1T^0$
σ_1	Maximum principal stress	$L^{-1}M^1T^{-2}$
$\sigma_{op,salt}$	Salt overpressure: vertical stress within salt in excess of integration of overburden	$L^{-1}M^1T^{-2}$
$\sigma_{v\ roof}$	Vertical stress acting on top of dome due to roof overburden	$L^{-1}M^1T^{-2}$
$\sigma_{v,salt}$	Measured vertical stress within the salt	$L^{-1}M^1T^{-2}$

Table B.2
Metric (SI) unit to English unit conversion.

Metric system	Conversion	English system
m	/0.3048	ft
kg	/0.4536	lb
N	/4.448	lbf
kPa	/6.895	psi
Pa	/47.88	psf
kN/m^3	/0.1572	pcf

References

Albertz, M., Beaumont, C., 2010. An investigation of salt tectonic structural styles in the Scotian Basin, offshore Atlantic Canada: 2. Comparison of observations with geometrically complex numerical models. Tectonics 29, TC4018.
Albertz, M., Beaumont, C., Shimeld, J.W., Ings, S.J., Gradmann, S., 2010. An investigation of salt tectonic structural styles in the Scotian Basin, offshore Atlantic Canada: 1. Comparison of observations with geometrically simple numerical models. Tectonics 29, TC4017.
Allen, J., Beaumont, C., 2012. Impact of inconsistent density scaling on physical analogue models of continental margin scale salt tectonics. J. Geophys. Res. Solid Earth 117, B08103.
Althaus, V.,E., 1977. A new model for fracture gradient. J. Can. Pet. Technol. 16, 98–108.
Bachrach, R., Sengupta, M., Salama, A., 2007. Stress and seismic anisotropy near salt bodies – numerical modeling and observation from wide-azimuth marine data. In: EAGE 69th Conference & Exhibition, London, UK.
Barnichon, J.D., Havenith, H., Hoffer, B., Charlier, R., Jongmans, D., Duchesne, J.C., 1999. The deformation of the Egersund-Ogna anorthosite massif, south Norway: finite-element modelling of diapirism. Tectonophysics 303, 109–130.
Beltrão, R.L.C., Sombra, C.L., Lage, A.C.V.M., Fagundes Netto, J.R., Henriques, C.C.D., 2009. Challenges and new technologies for the development of the pre-salt cluster, Santos Basin, Brazil. In: Offshore Technology Conference, Houston, Texas.
Bradley, W.B., 1978. Borehole Failure Near Salt Domes, Society of Petroleum Engineers Annual Fall Technical Conference and Exhibition. American Institute of Mining, Metallurgical, and Petroleum Engineers, Inc., Houston, Texas.
Chemia, Z., Schmeling, H., Koyi, H., 2009. The effect of the salt viscosity on future evolution of the Gorleben salt diapir, Germany. Tectonophysics 473, 446–456.
Crook, A.J.L., Willson, S.M., Yu, J.G., Owen, D.R.J., 2006. Predictive modelling of structure evolution in sandbox experiments. J. Struct. Geol. 28, 729–744.
Daudré, B., Cloetingh, S., 1994. Numerical modelling of salt diapirism: influence of the tectonic regime. Tectonophysics 240, 59–79.
Davis, T., Warner, M., Elders, C., Davison, I., 2000. Tertiary faulting patterns and growth history of Central Graben salt diapirs. In: Canadian Society of Exploratory Geophysicists, Annual Conf, p. 4. Abstracts (web publication).
Davison, I., Alsop, I., Birch, P., Elders, C., Evans, N., Nicholson, H., Rorison, P., Wade, D., Woodward, J., Young, M., 2000. Geometry and late-stage structural evolution of Central Graben salt diapirs, North Sea. Mar. Pet. Geol. 17, 499–522.
Dusseault, M.B., Maury, V., Sanfilippo, F., Santarelli, F.J., 2004. Drilling Around Salt: Risks, Stresses, and Uncertainties. American Rock Mechanics Association. Paper 04-647.
Fredrich, J.T., Coblentz, D., Fossum, A.F., Thorne, B.J., 2003. Stress perturbations adjacent to salt bodies in the deepwater Gulf of Mexico. In: Society of Petroleum Engineers Annual Technical Conference and Exhibition. 2003. Society of Petroleum Engineers, Denver, Colorado.
Fredrich, J.T., Fossum, A.F., Hickman, R.J., 2007. Mineralogy of deepwater Gulf of Mexico salt formations and implications for constitutive behavior. J. Pet. Sci. Eng. 57, 354–374.
Fullsack, P., 1995. An arbitrary Lagrangian–Eulerian formulation for creeping flows and its application in tectonic models. Geophys. J. Int. 120, 1–23.
Goteti, R., Ings, S.J., Beaumont, C., 2012. Development of salt minibasins initiated by sedimentary topographic relief. Earth Planet. Sci. Lett. 339/340, 103–116.
Gradmann, S., Beaumont, C., Albertz, M., 2009. Factors controlling the evolution of the Perdido Fold Belt, northwestern Gulf of Mexico, determined from numerical models. Tectonics 28, TC2002.
Jaeger, J.C., Cook, N.G.W., Zimmerman, R.W., 2007. Fundamentals of Rock Mechanics, fourth ed. Blackwell Publishing, Oxford, U.K.
Koupriantchik, D., Hunt, S.P., Boult, P.J., Meyers, A.G., 2005. Geomechanical modeling of salt diapirs: 3D salt structure from the Officer Basin, South Australia. In: Central Australian Basins Symposium.
Koupriantchik, D., Meyers, A.G., Hunt, S., 2004. 3D geomechanical modelling towards understanding stress anomalies causing wellbore instability. In: Gulf Rocks 2004, the 6th North America Rock Mechanics Symposium (NARMS). American Rock Mechanics Association, Houston, Texas.
Laubach, S.E., Eichhubl, P., Hilgers, C., Lander, R.H., 2010. Structural diagenesis. J. Struct. Geol. 32, 1866–1872.
Luo, G., Nikolinakou, M.A., Flemings, P.B., Hudec, M.R., 2012. Geomechanical modeling of stresses adjacent to salt bodies: 1. Uncoupled models. AAPG Bull. 96, 43–64.
Mackay, F., Inoue, N., Fontoura, S.A.B., Botelho, F., 2008. Geomechanical effects of a 3D vertical salt well drilling by FEA. In: The 42nd U.S. Rock Mechanics Symposium (USRMS). 2008. American Rock Mechanics Association, San Francisco, California.
Matthews, W.R., Kelly, J., 1967. How to predict formation pressure and fracture gradient. Oil Gas J. 20, 92–106.
Meyer, D., Zarra, D., Rains, D., Meltz, B., Hall, T., 2005. Emergence of the Lower Tertiary Wilcox trend in the deepwater Gulf of Mexico. World Oil, 72–77.
Muir Wood, D., 1990. Soil Behaviour and Critical State Soil Mechanics. Cambridge University Press, Cambridge, U.K.
Munson, D.E., 1997. Constitutive model of creep in rock salt applied to underground room closure. Int. J. Rock Mech. Mining Sci. 34, 233–247.

Munson, D.E., Dawson, P.R., 1979. Constitutive Model for the Low Temperature Creep of Salt (With Application to WIPP). SAND79-1853. Sandia National Laboratories, Albuquerque, NM.
Nikolinakou, M.A., Luo, G., Hudec, M.R., Flemings, P.B., 2012. Geomechanical modeling of stresses adjacent to salt bodies: 2. poro-elasto-plasticity and coupled overpressures. Am. Assoc. Pet. Geol. Bull. 96, 65–85.
Nygard, R., Gutierrez, M., Bratli, R.K., Hoeg, K., 2006. Brittle-ductile transition, shear failure and leakage in shales and mudrocks. Mar. Pet. Geol. 23, 201–212.
Nygard, R., Gutierrez, M., Gautam, R., Hoeg, K., 2004. Compaction behavior of argillaceous sediments as function of diagenesis. Mar. Pet. Geol. 21, 349–362.
O'Brien, J.J., Lerch, I., 1987. Modelling of the deformation and faulting of the formations overlying an uprising salt dome. In: Lerche, I., O'Brien, J.J. (Eds.), Dynamical Geology of Salt and Related Structures. Academic Press, London, pp. 419–455.
Orlic, B., Wassing, B.B.T., 2012. Modeling stress development and fault slip in producing hydrocarbon reservoirs Overlain by rock salt Caprocks. In: American Rock Mechanics Association 2012 Symposium p. Paper No 145.
Perez, M.A., Clyde, R., D'Ambrosio, P., Israel, R., Leavitt, T., Nutt, L., Johnson, C., Wiliamson, D., 2008. Meeting the subsalt challenge. Oilfield Rev. 20, 32–45.
Peric, D., Crook, A.J.L., 2004. Computational strategies for predictive geology with reference to salt tectonics. Comput. Methods Appl. Mech. Eng. 193, 5195–5222.
Pilkington, P.E., 1978. Fracture gradient estimates in tertiary basins. Pet. Eng. Int. 8, 138–148.
Poliakov, A.N.B., Podladchikov, Y., Talbot, C., 1993a. Initiation of salt diapirs with frictional overburdens: numerical experiments. Tectonophysics 228, 199–210.
Poliakov, A.N.B., Podladchikov, Y.Y., Dawson, E.C., Talbot, C.J., 1996. Salt Diapirism with Simultaneous Brittle Faulting and Viscous Flow. In: Geological Society, London, Special Publications 100, pp. 291–302.
Poliakov, A.N.B., van Balen, R., Podladchikov, Y., Daudre, B., Cloetingh, S., Talbot, C., 1993b. Numerical analysis of how sedimentation and redistribution of surficial sediments affects salt diapirism. Tectonophysics 226, 199–216.
Rockfield, 2010. ELFEN Forward Modeling User Manual. Rockfield Software Limited.
Rowan, M.G., Ratliff, R.A., 2012. Cross-section restoration of salt-related deformation: best practices and potential pitfalls. J. Struct. Geol. 41, 24–37.
Sanz, P.F., Dasari, G.R., 2010. Controls on in-situ stresses around salt bodies. In: Association, A.R.M. (Ed.), 44th US Rock Mechanics Symposium, Salt Lake City, UT June 27–30.
Schultz-Ela, D.D., 2003. Origin of drag folds bordering salt diapirs. AAPG Bull. 87, 757–780.
Schultz-Ela, D.D., Jackson, M.P.A., Vendeville, B.C., 1993. Mechanics of active salt diapirism. Tectonophysics 228, 275–312.
Seymour, K.P., Rae, G., Peden, J.M., Ormston, K., 1993. Drilling Close to Salt Diapirs in the North Sea, Offshore Europe. Society of Petroleum Engineers, Aberdeen, U.K.
Stewart, S.A., 2006. Implications of passive salt diapir kinematics for reservoir segmentation by radial and concentric faults. Mar. Pet. Geol. 23, 843–853.
Terzaghi, K., Peck, R.B., Mesri, G., 1996. Soil Mechanics in Engineering Practice. Wiley, New York.
Thornton, D.A., Roberts, D.T., Crook, A.J.L., Yu, J.G., 2011. Regional scale salt tectonics modelling: bench-scale validation and extension to field-scale problems. In: Beyond Balanced Sections: Geological Society of America Conference, Minneapolis, USA.
Turcotte, D.L., Schubert, G., 2002. Geodynamics. Cambridge University Press, Cambridge; U.K.
van-der-Zee, W., Ozan, C., Brudy, M., Holland, M., 2011. 3D geomechanical modeling of complex salt structures. In: SIMULIA Customer Conference.
Willson, S.M., Edwards, S., Heppard, P.D., Li, X., Coltrin, G., Chester, D.K., Harrison, H.L., Cocales, B.W., 2003. Wellbore stability challenges in the deep water, Gulf of Mexico: case history examples from the Pompano Field. In: SPE Annual Technical Conference and Exhibition. Society of Petroleum Engineers, Denver, Colorado.
Zerwer, A., 1994. Using Borehole Breakouts to Map Horizontal Stress Trajectories in the Gulf of Mexico (MSc thesis). Dept. of Earth Sci., University of Waterloo, p. 290.
Zoback, M.D., Healy, J.H., 1984. Friction, faulting and in situ stress. Ann. Geophys. 2, 689–698.